Punjab University Journal of Mathematics (2025), 57(05),504-533
https://doi.org/10.52280/pujm.2025.57(05)02

Development of Two-Step Fractional Iterative Technique of Convergence Order $(2\mu + 1)$ with Applications

Saima Akram
Department of Mathematics, Government College Women University Faisalabad, Faisalabad, 38000, Pakistan
Centre for Advanced Studies in Pure and Applied Mathematics, Bahauddin Zakariya University, Multan, 60000, Pakistan

Rida Batool
Department of Mathematics, Government College Women University Faisalabad, Faisalabad, 38000, Pakistan

*Faiza Akram
Centre for Advanced Studies in Pure and Applied Mathematics, Bahauddin Zakariya University, Multan, 60000, Pakistan

*Corresponding author
faiza4akram@gmail.com

Received
10 February, 2025

Accepted
06 July, 2025

Published Online
13 November, 2025

Abstract. Fractional iterative techniques possess the capability to model complex dynamic systems with greater accuracy, playing a crucial role in the advancement of numerical analysis. This study presents a novel class of advanced fractional iterative algorithms, developed to improve the efficiency and precision of solving challenging mathematical problems. Riemann-Liouville and Caputo fractional derivatives, with order (2μ) or $(\mu + 1)$, have been used in several recent publications to suggest single step fractional Newton-type approaches. In this article, we provide a two-step conformable fractional Newton-type approach with a $(2\mu + 1)$ convergence order employing the same derivatives. Convergence is analyzed, demonstrating its $(2\mu + 1)$ convergence. We conducted extensive analysis to evaluate the performance of our algorithm, focusing on absolute error and function evaluations at each iteration. The test functions used in these experiments span a wide range of applications in chemical sciences, civil engineering, and bacterial growth. The numerical outcomes support the theory and enhance the findings. The dynamical portraits reveal that the M_SFR method is a highly sensitive iterative approach, particularly effective for capturing complex dynamics.

AMS (MOS) Subject Classification Codes: 35S29; 40S70; 25U09
Key Words: Nonlinear equations, Fractional derivative, Fractional iterative scheme, Two-step method, Basins of attraction.

1. INTRODUCTION

Classical calculus is extended to fractional calculus, which handles derivatives of any order rather than simply whole integers. It is helpful for simulating complicated systems which are prevalent in fields like physics, biology, and engineering that possess memories or rely on previous actions. Fractional calculus is frequently utilized in a variety of disciplines to answer practical issues due to its versatility. Because they enable the refinement of solutions through repeated steps, iterative approaches are widely used techniques for solving nonlinear equations.

Riemann-Liouville Fractional Derivative [8]: Riemann-Liouville fractional derivative of a function $\Psi(\eta)$ of order μ, $0 < \mu \leq 1$ is defined as,

$$D^{\mu}_{a^+}\Psi(\eta) = \begin{cases} \frac{1}{\Gamma(1-\mu)} \frac{d}{d\eta} \int\limits_a^{\eta} \frac{\Psi(t)}{(\eta-t)^{\mu}}\, dt, & 0 < \mu \leq 1, \\ \frac{d\Psi(t)}{dt}, & \mu = 1. \end{cases}$$

This derivative does not holds the property of nonfractional derivative, $D^{\mu}_{a^+}C \neq 0$, where C is any constant.

The following theorem presents the Taylor series expansion of $f(x)$ involving the Riemann-Liouville derivative.

Theorem [9]: Assume the continuous function $\Psi : \mathbb{R} \to \mathbb{R}$ has fractional derivatives of order $k\mu$ for any positive integer k and any μ with $0 < \mu \leq 1$. Then, the following equality holds:

$$\Psi(\eta + h) = \sum_{k=0}^{\infty} \frac{h^{k\mu}}{\Gamma(k\mu + 1)}\, D^{k\mu}_{a+}\Psi(\eta),$$

where $D^{k\mu}_{a+}\Psi(\eta)$ is the Riemann-Liouville derivative of order $k\mu$ of $\Psi(\eta)$.

Caputo Fractional Derivative [8]: The Caputo fractional derivative of a function $\Psi(\eta)$ of order $\mu > 0$, with $a, \mu, \eta \in \mathbb{R}$, is defined as,

$$cD^{\mu}_{a}\Psi(\eta) = \begin{cases} \frac{1}{\Gamma(m-\mu)} \int\limits_a^{\eta} \frac{\Psi^{(m)}(t)}{(\eta-t)^{\mu+1-m}}\, dt, & m-1 < \mu \leq m \in \mathbb{N}, \\ \frac{d^m\Psi(\eta)}{d\eta^m}, & \mu = m \in \mathbb{N}. \end{cases}$$

This derivative satisfies the property of the non-fractional derivative: $cD^{\mu}_{a}C = 0$, where C is any constant.

Theorem [10]: Let us suppose that $cD^{\mu}_{a}\Psi(\eta) \in C([a, b])$ for $j = 1, 2, \ldots, n+1$ where $\mu \in (0, 1]$, then we have,

$$\Psi(\eta) = \sum_{i=0}^{n} cD^{i\mu}_{a}\Psi(a)\frac{(\eta - a)^{i\mu}}{\Gamma(i\mu + 1)} + cD^{(n+1)\mu}_{a}\Psi(\xi)\frac{(\eta - a)^{(n+1)\mu}}{\Gamma((n+1)\mu + 1)},$$

with $a \leq \xi \leq \eta$, for all $\eta \in (a, b]$ where $cD_a^{n\mu} = cD_a^{\mu} \cdot cD_a^{\mu} \cdot \cdots \cdot cD_a^{\mu}$ (n times).
These techniques provide fresh approaches to challenging issues that might not be addressed with conventional techniques when paired with fractional calculus. Both computing efficiency and accuracy are enhanced by this combination. Currently, there are very few fractional single-step iterative methods available in the literature, and only one two-step method has been developed so far see [1–4] and [11–13]. Recognizing the need for further advancements, we have designed a new two-step fractional iterative scheme that offers better results compared to the existing method.

In this work, in order to solve nonlinear equations, especially in scientific and engineering applications, we design and analyze a two-step fractional iterative strategy with convergence order of $2\mu + 1$. The new method's efficiency, convergence speed, and accuracy have been evaluated in comparison to other approaches. We utilize the approach to solve real-world issues, including beam deflection in chemical engineering, to demonstrate its value.

In 2019, Giro Candelario [5] developed the concept of a single-step fractional iterative process to a two-step method. He devised a two-step approach that requires one function and one fractional derivative value of a function $\Psi(\eta)$ of order μ in order to reach the $(2\mu + 1)th$ order of convergence.

$$\acute{Y_t} = \eta_t - \left(\Gamma(\mu + 1) \frac{\Psi(\eta_t)}{cD_{\tilde{\eta}}^{\mu} \Psi(\eta_t)} \right)^{\frac{1}{\mu}}, t = 0, 1, 2, ...,$$

$$\eta_{t+1} = \acute{Y_t} - \left(\Gamma(\mu + 1) \frac{\Psi(\acute{Y_t})}{cD_{\tilde{\eta}}^{\mu} \Psi(\eta_t)} \right)^{\frac{1}{\mu}}, t = 0, 1, 2, ...,$$

where $\Psi(\eta_t),\ \Psi(\acute{Y_t})$ represent functions of η_t and $\acute{Y_t}$ respectively, $cD_{\tilde{\eta}}^{\mu} \Psi(\eta_t)$ represents the Caputo fractional derivative of order μ, $\tilde{\eta}$ is the lower limit of fractional derivative and $0 < \mu \leq 1$. We thus provide a two-step fractional iterative strategy that is motivated by the research and the need to create $2\mu + 1$ order and more efficient convergence methods for roots utilizing fractional derivative. In comparison to the results of the previous schemes, the proposed scheme yields a wider region of convergence, better numerical results, and faster convergence. The remaining sections of the manuscript are arranged as follows:

In section 2 we used the Caputo and Riemann-Liouville fractional derivative to build an efficient $(2\mu + 1)$ order fractional iterative scheme, and then we analyzed its convergence to determine the order of convergence. In section 3, these specializations have been utilized to test the numerical findings and compare the performance of the newly constructed scheme with the previous schemes. In section 4, a graphical tool called the basin of attraction is used to illustrate the dynamic behavior of the family that is depicted on the complex plane. The concluding remarks are provided in section 5.

2. Methodology of Iterative Scheme

In this section, we develop a root-finding scheme of order $(2\mu + 1)$ for solving nonlinear equations involving fractional derivatives. The scheme is constructed as a two-step method.

We also present the evolution of the proposed scheme and provide a detailed convergence analysis using the Caputo fractional derivative.

This part builds a simple and efficient scheme for nonlinear equation roots that contain both Caputo fractional derivative and Riemann-Liouville derivative.

$$\acute{Y_t} = \eta_t - \left(\Gamma(\mu+1)\frac{\Psi(\eta_t)}{cD^{\mu}_{\eta^{\tilde{}}}\Psi(\eta_t)}\right)^{\frac{1}{\mu}}, t = 0,1,2,..$$

$$\eta_{t+1} = \acute{Y_t} - \left(\left(1-\mu\frac{\Psi(\acute{Y_t})}{\Psi(\acute{Y_t})+cD^{\mu}_{\eta^{\tilde{}}}\Psi(\eta_t)}\right)^{-1}\left(\Gamma(\mu+1)\frac{\Psi(\acute{Y_t})}{cD^{\mu}_{\eta^{\tilde{}}}\Psi(\eta_t)}\right)\right)^{\frac{1}{\mu}}, t = 0,1,2,... \tag{2. 1}$$

where $cD^{\mu}_{\eta^{\tilde{}}}\Psi(\eta_t)$ represents the Caputo fractional derivative of order μ.

The scheme in eq (2. 1) is a root finder schemes of order $(2\mu+1)$ for solving nonlinear equations with Caputo fractional derivatives, with order $\mu \in (0,1]$.

$$\acute{Y_t} = \eta_t - \left(\Gamma(\mu+1)\frac{\Psi(\eta_t)}{D^{\mu}_{a^+}\Psi(\eta_t)}\right)^{\frac{1}{\mu}}, t = 0,1,2,..$$

$$\eta_{t+1} = \acute{Y_t} - \left(\left(1-\mu\frac{\Psi(\acute{Y_t})}{\Psi(\acute{Y_t})+D^{\mu}_{a^+}\Psi(\eta_t)}\right)^{-1}\left(\Gamma(\mu+1)\frac{\Psi(\acute{Y_t})}{D^{\mu}_{a^+}\Psi(\eta_t)}\right)\right)^{\frac{1}{\mu}}, t = 0,1,2,... \tag{2. 2}$$

where $D^{\mu}_{a^+}\Psi(\acute{Y_t})$ represents the Riemann-Liouville derivative of order μ.

In the succeeding result, we proved that equation(2. 1) and equation(2. 2) attains the $(2\mu+1)$ order of convergence.

Theorem 2.1. *Let the continuous function $\Psi : D \subseteq \mathbb{R} \to \mathbb{R}$ has fractional derivative with order $t\mu$, for any positive integer t and any $\mu \in (0,1]$, in the interval D containing the zero $\eta^{\tilde{}}$ of $\Psi(\eta)$. Let us suppose $cD^{\mu}_{\eta^{\tilde{}}}\Psi(\eta)$ is continuous and not null at $\eta^{\tilde{}}$. If an initial approximation η_0 is sufficiently close to $\eta^{\tilde{}}$, then the local convergence order of the fractional newton method of Caputo type in equation(2. 1) is atleast $2\mu+1$, being $0 < \mu \leq 1$, and the error equation is,*

$$\begin{aligned} e_{t+1} = &\left(\frac{B}{\mu A^{1-1/\mu}C_2^{\mu-1}} + \frac{\Gamma(\frac{1}{\mu}+1)}{\Gamma(\frac{1}{\mu})}A\left(\frac{A\Gamma(2\mu+1)}{(\Gamma(\mu+1))^2} - B\right)\right)e_t^{2\mu+1} \\ &+ O\left(e_t^{\mu^2+2\mu+1}\right), t = 0,1,2,... \end{aligned} \tag{2. 3}$$

being

$$A = \left(\frac{\Gamma(2\mu+1) - (\Gamma(\mu+1))^2}{\mu\,(\Gamma(\mu+1))^2}\right)C_2^{\mu},$$

and

$$\begin{aligned} B &= \mu\left(\frac{\Gamma(2\mu+1)-(\Gamma(\mu+1))^2}{\mu(\Gamma(\mu+1))^2}\right)^{\mu-1} C_2^{\mu-1}\Big(\frac{1}{\mu}\Big(\frac{\Gamma(3\mu+1)-\Gamma(2\mu+1)(\Gamma(\mu+1))}{(\Gamma(2\mu+1))}C_3+ \\ &\quad \Gamma(2\mu+1)\frac{(\Gamma(\mu+1))^2-\Gamma(2\mu+1)}{(\Gamma(\mu+1))^3}C_2^2\Big)\Big)+ \\ &\quad \frac{1}{2\mu}\left(1-\frac{1}{\mu}\right)\left(\frac{(\Gamma(\mu+1))^2-\Gamma(2\mu+1)^2}{(\Gamma(\mu+1))^4}C_2^2\right). \end{aligned}$$

Proof. The Taylor expansion of $\Psi(\eta)$ and its Caputo-derivative at η_t around $\eta^{\tilde{}}$ can be expressed by

$$\Psi(\eta_t)=\frac{cD^{\mu}_{\eta^{\tilde{}}}\Psi(\eta^{\tilde{}})}{\Gamma(\mu+1)}\left[e_t^{\mu}+C_2e_t^{2\mu}+C_3e_t^{3\mu}+C_4e_t^{4\mu}\right]+O\left(e_t^{5\mu}\right), \tag{2. 4}$$

where η_t represents the error term and μ denotes the order and

$$\begin{aligned} cD^{\mu}_{\eta^{\tilde{}}}\Psi(\eta_t) &= \frac{cD^{\mu}_{\eta^{\tilde{}}}\Psi(\eta^{\tilde{}})}{\Gamma(\mu+1)}\Bigg[\Gamma(\mu+1)+\frac{\Gamma(2\mu+1)}{\Gamma(\mu+1)}C_2e_t^{\mu}+\frac{\Gamma(3\mu+1)}{\Gamma(2\mu+1)}C_3e_t^{2\mu}+\frac{\Gamma(4\mu+1)}{\Gamma(3\mu+1)} \\ &\quad C_4e_t^{3\mu}\Bigg]+O\left(e_t^{4\mu}\right). \end{aligned} \tag{2. 5}$$

$C_j=\frac{\Gamma(\mu+1)}{\Gamma(j\mu+1)}\frac{cD^{j\mu}_{\eta^{\tilde{}}}\Psi(\eta_t)}{cD^{\mu}_{\eta^{\tilde{}}}\Psi(\eta_t)}$for $j\geq 2$.

The quotient $\frac{\Psi(\eta_t)}{cD^{\mu}_{\eta^{\sim}}\Psi(\eta_t)}$ can be computed by dividing equation (2. 4) by equation (2. 5).

$$\begin{aligned} \frac{\Psi(\eta_t)}{cD^{\mu}_{\eta^{\sim}}\Psi(\eta_t)} &= \frac{1}{\Gamma(\mu+1)}e_t^{\mu}+\frac{(\Gamma(\mu+1))^2-\Gamma(2\mu+1)}{(\Gamma(\mu+1))^3}C_2^2e_t^{2\mu} \\ &\quad +\left(\frac{\Gamma(2\mu+1)\Gamma(\mu+1)-\Gamma(3\mu+1)}{\Gamma(2\mu+1)\Gamma(\mu+1)}C_3\right. \\ &\quad \left.-\frac{\Gamma(2\mu+1)}{\Gamma(\mu+1)}\left(\frac{(\Gamma(\mu+1))^2-\Gamma(2\mu+1)}{(\Gamma(\mu+1))^3}\right)C_2^2\right)e_t^{3\mu} \\ &\quad +O\left(e_t^{4\mu}\right), \end{aligned} \tag{2. 6}$$

Subsequently, multiplying the resulting expression by $\Gamma(\mu+1)$ yields:

$$\begin{aligned}\Gamma(\mu+1)\frac{\Psi(\eta_t)}{cD^{\mu}_{\eta\sim}\Psi(\eta_t)} &= e_t^{\mu}+\frac{\left(\Gamma(\mu+1)\right)^2-\Gamma(2\mu+1)}{\left(\Gamma(\mu+1)\right)^2}C_2^2e_t^{2\mu}\\ &+\left(\frac{\Gamma(2\mu+1)\Gamma(\mu+1)-\Gamma(3\mu+1)}{\Gamma(2\mu+1)}C_3\right.\\ &\left.-\Gamma(2\mu+1)\left(\frac{\left(\Gamma(\mu+1)\right)^2-\Gamma(2\mu+1)}{\left(\Gamma(\mu+1)\right)^3}\right)C_2^2\right)e_t^{3\mu}\\ &+O\left(e_t^{4\mu}\right).\end{aligned} \tag{2. 7}$$

Raising this expression to the power $\frac{1}{\mu}$:

$$\begin{aligned}\left(\Gamma(\mu+1)\frac{\Psi(\eta_t)}{cD^{\mu}_{\eta\sim}\Psi(\eta_t)}\right)^{\frac{1}{\mu}} &= e_t+\frac{1}{\mu}e_t^{1-\mu}\left(\left(\frac{\left(\Gamma(\mu+1)\right)^2-\Gamma(2\mu+1)}{\left(\Gamma(\mu+1)\right)^2}C_2e_t^{2\mu}\right)+\right.\\ &\left.\left(\frac{\Gamma(2\mu+1)\Gamma(\mu+1)-\Gamma(3\mu+1)}{\Gamma(2\mu+1)}C_3-\right.\right.\\ &\left.\left.\Gamma(2\mu+1)\frac{(\Gamma(\mu+1))^2-\Gamma(2\mu+1)}{\left(\Gamma(\mu+1)\right)^3}\right.\right.\\ &\left.\left.C_2^2\right)e_t^{3\mu}\right)+\frac{\Gamma(1/\mu+1)}{2\Gamma(1/\mu-1)}e_t^{1-2\mu}\\ &\left(\frac{\left(\Gamma(\mu+1)\right)^2-\Gamma(2\mu+1)}{\left(\Gamma(\mu+1)\right)^2}C_2e_t^{2\mu}\right)^2+\\ &O\left(e_t^{3\mu+1}\right).\end{aligned}$$

As $\Gamma(1/\mu+1)=\frac{1}{\mu}\Gamma(\mu+1)=\frac{1}{\mu}(\frac{1}{\mu}-1)\frac{1}{\mu}\Gamma(\frac{1}{\mu}-1)$,this implies that $\frac{\Gamma(\frac{1}{\mu}+1)}{2\Gamma(\frac{1}{\mu}-1)}=\frac{1}{2\mu}(\frac{1}{\mu}-1)$, and simplifying the expression yields:

$$\begin{aligned}\left(\Gamma(\mu+1)\frac{\Psi(\eta_t)}{cD^{\mu}_{\eta\sim}\Psi(\eta_t)}\right)^{\frac{1}{\mu}} &= e_t+\left(\frac{\left(\Gamma(\mu+1)\right)^2-\Gamma(2\mu+1)}{\mu\left(\Gamma(\mu+1)\right)^2}\right)C_2e_t^{\mu+1}\\ &+\left(\frac{1}{\mu}\left(\frac{\Gamma(2\mu+1)\Gamma(\mu+1)}{\Gamma(2\mu+1)}-\frac{\Gamma(3\mu+1)}{\Gamma(2\mu+1)}C_3\right)\right.\\ &\left.+\Gamma(2\mu+1)\frac{\Gamma(2\mu+1)-(\Gamma(\mu+1))^2}{\left(\Gamma(\mu+1)\right)^3}C_2^2\right.\\ &\left.+\frac{1}{2\mu}\left(\frac{1}{\mu}-1\right)\left(\frac{(\Gamma(\mu+1))^2-\Gamma(2\mu+1)^2}{\left(\Gamma(\mu+1)\right)^4}\right)C_2^2\right)e_t^{2\mu+1}\\ &+O\left(e_t^{3\mu+1}\right).\end{aligned} \tag{2. 8}$$

Let $e_t = \eta_t - \eta^{\sim}$, we can then state that:

$$\begin{aligned}
\acute{Y_t} &= \eta^{\hat{}} - \left(\frac{(\Gamma(\mu+1))^2 - \Gamma(2\mu+1)}{\mu\,(\Gamma(\mu+1))^2} \right) C_2 e_t^{\mu+1} \\
&\quad - \left(\frac{1}{\mu} \frac{\Gamma(2\mu+1)\Gamma(\mu+1) - \Gamma(3\mu+1)}{\Gamma(2\mu+1)} C_3 \right. \\
&\quad \left. + \Gamma(2\mu+1) \frac{\Gamma(2\mu+1) - (\Gamma(\mu+1))^2}{(\Gamma(\mu+1))^3} C_2^2 \right) e_t^{2\mu+1} \\
&\quad + \frac{1}{2\mu} \left(\frac{1}{\mu} - 1 \right) \left(\frac{(\Gamma(\mu+1))^2 - \Gamma(2\mu+1)^2}{(\Gamma(\mu+1))^4} \right) C_2^2 e_t^{3\mu+1} \\
&\quad + O\left(e_t^{3\mu+1} \right). \qquad (2.\ 9)
\end{aligned}$$

Let us evaluate $\Psi(\acute{Y_t})$.

$$\Psi(\acute{Y_t}) = \frac{c D^{\mu}_{\eta^{\hat{}}} \Psi(\eta_t)}{\Gamma(\mu+1)} \left[\left(\acute{Y_t} - \eta^{\hat{}} \right)^{\mu} + C_2 \left(\acute{Y_t} - \eta^{\hat{}} \right)^{2\mu} \right] + O\left(e_t^{3\mu} \right). \qquad (2.\ 10)$$

By substituting equation (2. 9) into equation (2. 10), we get:

$$\begin{aligned}
\left(\acute{Y_t} - \eta^{\hat{}} \right)^{\mu} &= \left(\frac{\Gamma(2\mu+1) - (\Gamma(\mu+1))^2}{\mu\,(\Gamma(\mu+1))^2} C_2 e_t^{\mu+1} \right. \\
&\quad + \left(\frac{1}{\mu} \left(\frac{\Gamma(3\mu+1) - \Gamma(2\mu+1)\Gamma(\mu+1)}{\Gamma(2\mu+1)} C_3 \right. \right. \\
&\quad \left. \left. + \Gamma(2\mu+1) \frac{(\Gamma(\mu+1))^2 - \Gamma(2\mu+1)}{(\Gamma(\mu+1))^3} C_2^2 \right) \right) \\
&\quad \left. + \left(\frac{1}{2\mu} \left(\frac{1}{\mu} - 1 \right) \left(\frac{(\Gamma(\mu+1))^2 - \Gamma(2\mu+1)^2}{(\Gamma(\mu+1))^4} \right) C_2^2 e_t^{2\mu+1} \right)^{\mu} \right. \\
&\quad + O\left(e_t^{\mu^2+3\mu} \right).
\end{aligned}$$

$$\begin{aligned}\left(\acute{Y}_t-\eta^{\sim}\right)^{\mu} &= \left(\frac{\Gamma(2\mu+1)-(\Gamma(\mu+1))^2}{\mu\left(\Gamma(\mu+1)\right)^2}\right)^{\mu} C_2^{\mu} e_t^{\mu^2+\mu} \\ &+\mu\left(\frac{\Gamma(2\mu+1)-(\Gamma(\mu+1))^2}{\mu\left(\Gamma(\mu+1)\right)^2}\right)^{\mu-1} C_2^{\mu-1} e_t^{\mu^2-1} \\ &\left(\frac{1}{\mu}\left(\frac{\Gamma(3\mu+1)-\Gamma(2\mu+1)\Gamma(\mu+1)}{\Gamma(2\mu+1)}C_3\right.\right. \\ &\left.\left.+\Gamma(2\mu+1)\frac{(\Gamma(\mu+1))^2-\Gamma(2\mu+1)}{(\Gamma(\mu+1))^3}C_2^2\right)\right) \\ &+\frac{1}{2\mu}\left(1-\frac{1}{\mu}\right)\left(\frac{(\Gamma(\mu+1))^2-\Gamma(2\mu+1)^2}{(\Gamma(\mu+1))^4}\right)C_2^2 e_t^{2\mu+1} \\ &+O\left(e_t^{\mu^2+3\mu}\right).\end{aligned}$$

by simplifying:

$$\begin{aligned}\left(\acute{Y}_t-\eta^{\sim}\right)^{\mu} &= \left(\frac{\Gamma(2\mu+1)-(\Gamma(\mu+1))^2}{\mu\left(\Gamma(\mu+1)\right)^2}\right)^{\mu} C_2^{\mu} e_t^{\mu^2+\mu} \\ &+\mu\left(\frac{\Gamma(2\mu+1)-(\Gamma(\mu+1))^2}{\mu\left(\Gamma(\mu+1)\right)^2}\right)^{\mu-1} C_2^{\mu-1}\left(\frac{1}{\mu}\right. \\ &\left.\left(\frac{\Gamma(3\mu+1)-\Gamma(2\mu+1)\Gamma(\mu+1)}{\Gamma(2\mu+1)}C_3+\Gamma(2\mu+1)\frac{(\Gamma(\mu+1))^2-\Gamma(2\mu+1)}{(\Gamma(\mu+1))^3}\right.\right. \\ &\left.\left.C_2^2\right)\right)+\frac{1}{2\mu}\left(1-\frac{1}{\mu}\right)\left(\frac{(\Gamma(\mu+1))^2-\Gamma(2\mu+1)^2}{(\Gamma(\mu+1))^4}\right)C_2^2 e_t^{\mu^2+2\mu}+O\left(e_t^{\mu^2+3\mu}\right).\end{aligned} \tag{2. 11}$$

We can see that $\mu^2+3\mu \geq \mu$ for all $\mu \in [0,1]$. It is also clear that if we choose the first term of the expansion $C_2\left(\acute{Y}_t-\eta^{\sim}\right)^{2\mu}$, it will have order $(\mu+1)\,2\mu = 2\mu^2+2\mu \geq 3\mu$ for all $\mu \in [0.5,1]$. Therefore, by substituting equation (2. 11) into equation (2. 10), we

get:

$$\begin{aligned}\Psi(\acute{Y}_t) &= \frac{cD^{\mu}_{\eta^-}\Psi(\eta_t)}{\Gamma(\mu+1)}\Bigg[\left(\frac{\Gamma(2\mu+1)-(\Gamma(\mu+1))^2}{\mu\,(\Gamma(\mu+1))^2}\right)^{\mu} C_2^{\mu} e_t^{\mu^2+\mu} + \\ &\mu\left(\frac{\Gamma(2\mu+1)-(\Gamma(\mu+1))^2}{\mu\,(\Gamma(\mu+1))^2}\right)^{\mu-1} \\ &C_2^{\mu-1}\Bigg(\frac{1}{\mu}\Bigg(\frac{\Gamma(3\mu+1)-\Gamma(2\mu+1)\Gamma(\mu+1)}{\Gamma(2\mu+1)}C_3 \\ &+\Gamma(2\mu+1)\frac{(\Gamma(\mu+1))^2-\Gamma(2\mu+1)}{(\Gamma(\mu+1))^3}C_2^2\Bigg) \\ &+\frac{1}{2\mu}\left(1-\frac{1}{\mu}\right)\left(\frac{(\Gamma(\mu+1))^2-\Gamma(2\mu+1)^2}{(\Gamma(\mu+1))^4}\right)C_2^2 \\ &\Bigg)e_t^{\mu^2+2\mu}\Bigg] + O\left(e_t^{\mu^2+3\mu}\right).\end{aligned}$$

Let us call:

$$A = \left(\frac{\Gamma(2\mu+1)-(\Gamma(\mu+1))^2}{\mu\,(\Gamma(\mu+1))^2}\right)^{\mu} C_2^{\mu},$$

and

$$\begin{aligned}B &= \mu\left(\frac{\Gamma(2\mu+1)-(\Gamma(\mu+1))^2}{\mu\,(\Gamma(\mu+1))^2}\right)^{\mu-1} \\ &C_2^{\mu-1}\Bigg(\Bigg(\frac{1}{\mu}(\frac{\Gamma(3\mu+1)-\Gamma(2\mu+1)\,(\Gamma(\mu+1))}{(\Gamma(2\mu+1))}C_3+\Gamma(2\mu+1)\frac{(\Gamma(\mu+1))^2-\Gamma(2\mu+1)}{(\Gamma(\mu+1))^3} \\ &C_2^2\Bigg)+\frac{1}{2\mu}\left(1-\frac{1}{\mu}\right)\left(\frac{(\Gamma(\mu+1))^2-\Gamma(2\mu+1)^2}{(\Gamma(\mu+1))^4}C_2^2\right)\Bigg).\end{aligned}$$

then,

$$\Psi(\acute{Y}_t) = \frac{cD^{\mu}_{\eta^-}\Psi(\eta_t)}{\Gamma(\mu+1)}\left[Ae_t^{\mu^2+\mu} + Be_t^{\mu^2+2\mu}\right] + O\left(e_t^{\mu^2+3\mu}\right). \tag{2. 12}$$

The quotient $\frac{\Psi(\acute{Y}_t)}{cD^{\mu}_{\eta^-}\Psi(\eta_t)}$ results:

$$\frac{\Psi(\acute{Y}_t)}{cD^{\mu}_{\eta^-}\Psi(\eta_t)} = \frac{Ae_t^{\mu^2+\mu}}{\Gamma(\mu+1)} + \frac{1}{\Gamma(\mu+1)}\left(B - \frac{A\Gamma(2\mu+1)}{(\Gamma(\mu+1))^2}\right)e_t^{\mu^2+2\mu} + O\left(e_t^{\mu^2+3\mu}\right). \tag{2. 13}$$

By adding equation(2. 12) and equation(2. 5), we get:

$$\Psi(\acute{Y}_t)+cD^{\mu}_{\tilde{\eta}}\Psi(\eta_t) = \frac{cD^{\mu}_{\tilde{\Psi}}\Psi(\tilde{\eta})}{\Gamma(\mu+1)}\left[Ae_t^{\mu^2+\mu}+Be_t^{\mu^2+2\mu}+\Gamma(\mu+1)+\frac{\Gamma(2\mu+1)}{\Gamma(\mu+1)}C_2e_t^{\mu}+\frac{\Gamma(3\mu+1)}{\Gamma(2\mu+1)}C_3e_t^{2\mu}+\frac{\Gamma(4\mu+1)}{\Gamma(3\mu+1)}C_4e_t^{3\mu}\right]+O\left(e_t^{4\mu}\right). \quad (2.\ 14)$$

Dividing equation(2. 5) by equation(2. 14):

$$\frac{\Psi(\acute{Y}_t)}{\Psi(\acute{Y}_t)+cD^{\mu}_{\tilde{\eta}}\Psi(\eta_t)} = \left(Ae_t^{\mu^2+\mu}+Be_t^{\mu^2+2\mu}\right)\frac{1}{\Gamma(\mu+1)}\left(1+\frac{Ae_t^{\mu^2+\mu}}{\Gamma(\mu+1)}+\frac{Be_t^{\mu^2+2\mu}}{\Gamma(\mu+1)}+\frac{\Gamma(2\mu+1)}{(\Gamma(\mu+1))^2}C_2e_t^{\mu}+\frac{\Gamma(3\mu+1)}{(\Gamma(\mu+1))\,(\Gamma(2\mu+1))}C_3e_t^{2\mu}+\frac{\Gamma(4\mu+1)}{(\Gamma(\mu+1))\,(\Gamma(3\mu+)\,1)}C_4e_t^{3\mu}\right)^{-1}.$$

$$\frac{\Psi(\acute{Y}_t)}{\Psi(\acute{Y}_t)+cD^{\mu}_{\tilde{\eta}}\Psi(\eta_t)} = \left(Ae_t^{\mu^2+\mu}+Be_t^{\mu^2+2\mu}\right)\frac{1}{\Gamma(\mu+1)}\left(1-\frac{Ae_t^{\mu^2+\mu}}{\Gamma(\mu+1)}-\frac{Be_t^{\mu^2+2\mu}}{\Gamma(\mu+1)}-\frac{\Gamma(2\mu+1)}{(\Gamma(\mu+1))^2}C_2e_t^{\mu}-\frac{\Gamma(3\mu+1)}{(\Gamma(\mu+1))\,(\Gamma(2\mu+1))}C_3e_t^{2\mu}-\frac{\Gamma(4\mu+1)}{(\Gamma(\mu+1))\,(\Gamma(3\mu+)\,1)}C_4e_t^{3\mu}\right).$$

$$\frac{\Psi(\acute{Y}_t)}{\Psi(\acute{Y}_t)+cD^{\mu}_{\tilde{\eta}}\Psi(\eta_t)} = \left(Ae_t^{\mu^2+\mu}+Be_t^{\mu^2+2\mu}-\frac{A^2e_t^{2\mu^2+2\mu}}{\Gamma(\mu+1)}-\frac{ABe_t^{2\mu^2+3\mu}}{\Gamma(\mu+1)}-\frac{ABe_t^{2\mu^2+3\mu}}{\Gamma(\mu+1)}-\frac{B^2e_t^{2\mu^2+4\mu}}{\Gamma(\mu+1)}-\frac{\Gamma(2\mu+1)}{\Gamma(\mu+1)^2}AC_2e_t^{\mu^2+2\mu}-\frac{\Gamma(2\mu+1)}{\Gamma(\mu+1)^2}BC_2e_t^{\mu^2+3\mu}-\frac{\Gamma(3\mu+1)}{\Gamma(2\mu+1)\Gamma(\mu+1)}AC_3e_t^{\mu^2+3\mu}-\frac{\Gamma(3\mu+1)}{\Gamma(2\mu+1)\Gamma(\mu+1)}BC_3e_t^{\mu^2+3\mu}-\frac{\Gamma(4\mu+1)}{\Gamma(3\mu+1)\Gamma(\mu+1)}AC_4e_t^{\mu^2+4\mu}\right)\left(\frac{1}{\Gamma(\mu+1)}\right)+O\left(e_t^{\mu^2+5\mu}\right).$$

$$\frac{\Psi(\acute{Y}_t)}{\Psi(\acute{Y}_t)+cD^{\mu}_{\tilde{\eta}}\Psi(\eta_t)} = \left(Ae_t^{\mu^2+\mu}+\left(B-\frac{\Gamma(2\mu+1)}{(\Gamma(\mu+1))^2}AC_2\right)e_t^{\mu^2+2\mu}-\frac{A^2e_t^{2\mu^2+2\mu}}{\Gamma(\mu+1)}\right)\left(\frac{1}{\Gamma(\mu+1)}\right)+O\left(e_t^{\mu^2+3\mu}\right). \quad (2.\ 15)$$

Multiplying μ on both sides of equation(2. 15):

$$\mu\frac{\Psi(\acute{Y}_t)}{\Psi(\acute{Y}_t)+cD^{\mu}_{\eta^-}\Psi(\eta_t)} = \left(\frac{\mu Ae_t^{\mu^2+\mu}}{\Gamma(\mu+1)}+\frac{\mu}{\Gamma(\mu+1)}\left(B-\frac{\Gamma(2\mu+1)}{\Gamma(\mu+1)^2}AC_2\right)e_t^{\mu^2+2\mu} -\frac{\mu A^2e_t^{2\mu^2+2\mu}}{\Gamma(\mu+1)}\right)+O\left(e_t^{\mu^2+3\mu}\right).$$

$$1-\mu\frac{\Psi(\acute{Y}_t)}{\Psi(\acute{Y}_t)+cD^{\mu}_{\eta^-}\Psi(\eta_t)} = \left(1-\frac{\mu Ae_t^{\mu^2+\mu}}{\Gamma(\mu+1)}+\frac{\mu}{\Gamma(\mu+1)}\left(B-\frac{\Gamma(2\mu+1)}{\Gamma(\mu+1)^2}AC_2\right)e_t^{\mu^2+2\mu} -\frac{\mu A^2e_t^{2\mu^2+2\mu}}{\Gamma(\mu+1)}\right)+O\left(e_t^{\mu^2+3\mu}\right). \quad (2.\ 16)$$

Raising the expression equation(2. 16) to power -1.

$$\left(1-\mu\frac{\Psi(\acute{Y}_t)}{\Psi(\acute{Y}_t)+cD^{\mu}_{\eta^-}\Psi(\eta_t)}\right)^{-1} = \left(1-\frac{\mu Ae_t^{\mu^2+\mu}}{\Gamma(\mu+1)}+\frac{\mu}{\Gamma(\mu+1)}\left(B-\frac{\Gamma(2\mu+1)}{\Gamma(\mu+1)^2}AC_2\right) e_t^{\mu^2+2\mu}-\frac{\mu A^2e_t^{2\mu^2+2\mu}}{\Gamma(\mu+1)}+O\left(e_t^{\mu^2+3\mu}\right)\right)^{-1}.$$

By using the binomial expansion, we get the results:

$$\left(1-\mu\frac{\Psi(\acute{Y}_t)}{\Psi(\acute{Y}_t)+cD^{\mu}_{\eta^-}\Psi(\eta_t)}\right)^{-1} = 1+\frac{\mu Ae_t^{\mu^2+\mu}}{\Gamma(\mu+1)}-\frac{\mu}{\Gamma(\mu+1)}\left(B-\frac{\Gamma(2\mu+1)}{\Gamma(\mu+1)^2}AC_2\right) e_t^{\mu^2+2\mu}+\frac{\mu A^2e_t^{2\mu^2+2\mu}}{\Gamma(\mu+1)}. \quad (2.\ 17)$$

Now multiplying by $\Gamma(\mu+1)$ with equation(2. 13).

$$\Gamma(\mu+1)\frac{\Psi(\acute{Y}_t)}{cD^{\mu}_{\eta^-}\Psi(\eta_t)} = Ae_t^{\mu^2+\mu}+\left(B-\frac{A\Gamma(2\mu+1)}{(\Gamma(\mu+1))^2}\right)e_t^{\mu^2+2\mu}+ O\left(e_t^{\mu^2+3\mu}\right). \quad (2.\ 18)$$

Now, by multiplying equation (2. 17) and equation (2. 18), we get:

$$\left(1-\mu\frac{\Psi(\acute{Y}_t)}{\Psi(\acute{Y}_t)+cD^{\mu}_{\eta^{\text{-}}}\Psi(\eta_t)}\right)^{-1}\left(\Gamma(\mu+1)\frac{\Psi(\acute{Y}_t)}{cD^{\mu}_{\eta^{\text{-}}}\Psi(\eta_t)}\right) = \left(1+\frac{\mu Ae_t^{\mu^2+\mu}}{\Gamma(\mu+1)}-\frac{\mu}{\Gamma(\mu+1)}\left(B-\frac{\Gamma(2\mu+1)}{\Gamma(\mu+1)^2}AC_2\right)e_t^{\mu^2+2\mu}+\frac{\mu A^2e_t^{2\mu^2+2\mu}}{\Gamma(\mu+1)}\right)\left(Ae_t^{\mu^2+\mu}+\left(B-\frac{A\Gamma(2\mu+1)}{(\Gamma(\mu+1))^2}\right)e_t^{\mu^2+2\mu}\right).$$

By simplifying,

$$\left(1-\mu\frac{\Psi(\acute{Y}_t)}{\Psi(\acute{Y}_t)+cD^{\mu}_{\eta^{\text{-}}}\Psi(\eta_t)}\right)^{-1}\left(\Gamma(\mu+1)\frac{\Psi(\acute{Y}_t)}{cD^{\mu}_{\eta^{\text{-}}}\Psi(\eta_t)}\right) = Ae_t^{\mu^2+\mu}+\left(B-\frac{A\Gamma(2\mu+1)}{(\Gamma(\mu+1))^2}\right)e_t^{\mu^2+2\mu}+\mu A^2e_t^{2\mu^2+2\mu}+\mu Ae_t^{\mu^2+\mu}\left(B-\frac{A\Gamma(2\mu+1)}{(\Gamma(\mu+1))^2}\right)e_t^{\mu^2+2\mu}-\frac{A\mu}{\Gamma(\mu+1)}\left(B-\frac{AC_2\Gamma(2\mu+1)}{(\Gamma(\mu+1))^2}\right)e_t^{\mu^2+2\mu}\left(Ae_t^{\mu^2+\mu}\right)-\frac{\mu}{\Gamma(\mu+1)}\left(B-\frac{AC_2\Gamma(2\mu+1)}{(\Gamma(\mu+1))^2}\right)e_t^{\mu^2+2\mu}\left(B-\frac{A\Gamma(2\mu+1)}{(\Gamma(\mu+1))^2}\right)e_t^{\mu^2+2\mu}.$$

$$
\begin{aligned}
= \quad & Ae_t^{\mu^2+\mu} + \left(B - \frac{A\Gamma(2\mu+1)}{(\Gamma(\mu+1))^2}\right) e_t^{\mu^2+2\mu} + \mu A^2 e_t^{2\mu^2+2\mu} + \\
& \mu A \left(B - \frac{A\Gamma(2\mu+1)}{(\Gamma(\mu+1))^2}\right) e_t^{2\mu^2+3\mu} - \frac{\mu A}{\Gamma(\mu+1)} \\
& \left(B - \frac{AC_2\Gamma(2\mu+1)}{(\Gamma(\mu+1))^2}\right) e_t^{2\mu^2+3\mu}.
\end{aligned}
$$

$$
\begin{aligned}
\left(1 - \mu\frac{\Psi(\acute{Y}_t)}{\Psi(\acute{Y}_t) + cD_{\eta^-}^{\mu}\Psi(\eta_t)}\right)^{-1} \left(\Gamma(\mu+1)\frac{\Psi(\acute{Y}_t)}{cD_{\eta^-}^{\mu}\Psi(\eta_t)}\right) \quad = \quad & Ae_t^{\mu^2+\mu} + \left(B - \frac{A\Gamma(2\mu+1)}{(\Gamma(\mu+1))^2}\right) \\
& e_t^{\mu^2+2\mu} + \mu A^2 e_t^{2\mu^2+2\mu} + \\
& \mu A \left(B - \frac{A\Gamma(2\mu+1)}{(\Gamma(\mu+1))^2}\right) \\
& e_t^{2\mu^2+3\mu} - \frac{\mu A}{\Gamma(\mu+1)} \\
& \left(B - \frac{AC_2\Gamma(2\mu+1)}{(\Gamma(\mu+1))^2}\right) \\
& e_t^{2\mu^2+3\mu}.
\end{aligned}
$$

Raising this expression to the power $\frac{1}{\mu}$:

$$
\begin{aligned}
\left(\left(1 - \mu\frac{\Psi(\acute{Y}_t)}{\Psi(\acute{Y}_t) + cD_{\eta^-}^{\mu}\Psi(\eta_t)}\right)^{-1} \left(\Gamma(\mu+1)\frac{\Psi(\acute{Y}_t)}{cD_{\eta^-}^{\mu}\Psi(\eta_t)}\right)\right)^{\frac{1}{\mu}} \quad = \quad & A^{\frac{1}{\mu}} e_t^{\mu+1} + \frac{\Gamma(\frac{1}{\mu}+1)}{\Gamma(\frac{1}{\mu})} Ae_t^{1-\mu^2} \\
& \left[\left(B - \frac{A\Gamma(2\mu+1)}{(\Gamma(\mu+1))^2}\right)\right. \\
& e_t^{\mu^2+2\mu} + \mu A^2 e_t^{2\mu^2+2\mu} + \\
& \mu A \left(B - \frac{A\Gamma(2\mu+1)}{(\Gamma(\mu+1))^2}\right) \\
& e_t^{2\mu^2+3\mu} - \frac{\mu A}{\Gamma(\mu+1)} \\
& \left(B - \frac{AC_2\Gamma(2\mu+1)}{(\Gamma(\mu+1))^2}\right) \\
& \left. e_t^{2\mu^2+3\mu}\right].
\end{aligned}
$$

$$\left(\left(1-\mu\frac{\Psi(\acute{Y}_t)}{\Psi(\acute{Y}_t)+cD^{\mu}_{\eta^-}\Psi(\eta_t)}\right)^{-1}\left(\Gamma(\mu+1)\frac{\Psi(\acute{Y}_t)}{cD^{\mu}_{\eta^-}\Psi(\eta_t)}\right)\right)^{\frac{1}{\mu}} = A^{\frac{1}{\mu}}e_t^{\mu+1}+\frac{\Gamma(\frac{1}{\mu}+1)}{\Gamma(\frac{1}{\mu})}Ae_t^{1-\mu^2}$$
$$\left[\left(B-\frac{A\Gamma(2\mu+1)}{(\Gamma(\mu+1))^2}\right)\right.$$
$$e_t^{\mu^2+2\mu}+\mu A^2e_t^{2\mu^2+2\mu}+$$
$$\mu A\left(B-\frac{A\Gamma(2\mu+1)}{(\Gamma(\mu+1))^2}\right)$$
$$e_t^{2\mu^2+3\mu}-\frac{\mu A}{\Gamma(\mu+1)}$$
$$\left(B-\frac{AC_2\Gamma(2\mu+1)}{(\Gamma(\mu+1))^2}\right)$$
$$\left.e_t^{2\mu^2+3\mu}\right]+O\left(e_t^{2\mu^2+4\mu}\right).$$

Let

$$\left(\left(1-\mu\frac{\Psi(\acute{Y}_t)}{\Psi(\acute{Y}_t)+cD^{\mu}_{\eta^-}\Psi(\eta_t)}\right)^{-1}\left(\Gamma(\mu+1)\frac{\Psi(\acute{Y}_t)}{cD^{\mu}_{\eta^-}\Psi(\eta_t)}\right)\right)^{\frac{1}{\mu}} = A^{\frac{1}{\mu}}e_t^{\mu+1}+\frac{\Gamma(\frac{1}{\mu}+1)}{\Gamma(\frac{1}{\mu})}A$$
$$\left(B-\frac{A\Gamma(2\mu+1)}{(\Gamma(\mu+1))^2}\right)e_t^{2\mu+1}$$
$$+\frac{\Gamma(\frac{1}{\mu}+1)}{\Gamma(\frac{1}{\mu})}\mu A^3e_t^{\mu^2+2\mu+1}$$
$$-\frac{\Gamma(\frac{1}{\mu}+1)}{\Gamma(\frac{1}{\mu})}$$
$$\mu A\left(B-\frac{A\Gamma(2\mu+1)}{(\Gamma(\mu+1))^2}\right)$$
$$e_t^{\mu^2+3\mu+1}-\frac{\mu A}{\Gamma(\mu+1)}$$
$$\left(B-\frac{AC_2\Gamma(2\mu+1)}{(\Gamma(\mu+1))^2}\right)$$
$$\left.e_t^{1+\mu^2+3\mu}\right]+O\left(e_t^{1+\mu^2+4\mu}\right).$$

$$
\begin{aligned}
e_{t+1}+\eta^{\tilde{}} &= e_t+\eta^{\tilde{}}+\left[-e_t+A^{1/\mu}e_t^{\mu+1}+\left(\frac{B}{\mu A^{1-1/\mu}C_2^{\mu-1}}\right)e_t^{2\mu+1}\right]- \\
&\left[A^{\frac{1}{\mu}}e_t^{\mu+1}+\frac{\Gamma(\frac{1}{\mu}+1)}{\Gamma(\frac{1}{\mu})}A\left(B-\frac{A\Gamma(2\mu+1)}{(\Gamma(\mu+1))^2}\right)e_t^{2\mu+1}+\right. \\
&\frac{\Gamma(\frac{1}{\mu}+1)}{\Gamma(\frac{1}{\mu})}\mu A^3e_t^{\mu^2+2\mu+1}-\frac{\Gamma(\frac{1}{\mu}+1)}{\Gamma(\frac{1}{\mu})} \\
&\mu A\left(B-\frac{A\Gamma(2\mu+1)}{(\Gamma(\mu+1))^2}\right)e_t^{\mu^2+3\mu+1}-\frac{\mu A}{\Gamma(\mu+1)} \\
&\left.\left(B-\frac{AC_2\Gamma(2\mu+1)}{(\Gamma(\mu+1))^2}\right)e_t^{1+\mu^2+3\mu}\right]+O\left(e_t^{1+\mu^2+4\mu}\right).
\end{aligned}
$$

Therefore,

$$
e_{t+1}=\left(\frac{B}{\mu A^{1-1/\mu}C_2^{\mu-1}}+\frac{\Gamma(\frac{1}{\mu}+1)}{\Gamma(\frac{1}{\mu})}A\left(\frac{A\Gamma(2\mu+1)}{(\Gamma(\mu+1))^2}-B\right)\right)e_t^{2\mu+1}+O\left(e_t^{\mu^2+2\mu+1}\right).
$$

□

Theorem 2.2. *Let the continuous function $\Psi : D \subseteq \mathbb{R} \to \mathbb{R}$ has fractional derivative with order $t\mu$, for any positive integer t and any $\mu \in (0,1]$, in the interval D containing the zero $\eta^{\tilde{}}$ of $\Psi(\eta)$. Let us suppose $cD^{\mu}_{\eta^{\tilde{}}}\Psi(\eta)$ is continuous and not null at $\eta^{\tilde{}}$. If an initial approximation η_0 is sufficiently close to $\eta^{\tilde{}}$, then the local convergence order of the fractional newton method with Riemann-Liouville derivative in equation(2. 2).*

$$
\acute{Y_t}=\eta_t-\left(\Gamma(\mu+1)\frac{\Psi(\eta_t)}{D^{\mu}_{a^+}\Psi(\eta_t)}\right)^{\frac{1}{\mu}},t=0,1,2,...
$$

$$
\eta_{t+1}=\acute{Y_t}-\left(\left(1-\mu\frac{\Psi(\acute{Y_t})}{\Psi(\acute{Y_t})+D^{\mu}_{a^+}\Psi(\acute{Y})}\right)^{-1}\left(\Gamma(\mu+1)\frac{\Psi(\acute{Y_t})}{D^{\mu}_{a^+}\Psi(\acute{Y})}\right)\right)^{\frac{1}{\mu}},t=0,1,2,... \tag{2. 19}
$$

The convergence order is at least $2\mu+1$, with $0<\mu\leq 1$, and the error equation is:

$$
e_{t+1}=\left(\frac{B}{\mu A^{1-1/\mu}C_2^{\mu-1}}+\frac{\Gamma(\frac{1}{\mu}+1)}{\Gamma(\frac{1}{\mu})}A\left(\frac{A\Gamma(2\mu+1)}{(\Gamma(\mu+1))^2}-B\right)\right)e_t^{2\mu+1}+O\left(e_t^{\mu^2+2\mu+1}\right),t=0,1,2,... \tag{2. 20}
$$

$$
A=\left(\frac{\Gamma(2\mu+1)-(\Gamma(\mu+1))^2}{\mu\left(\Gamma(\mu+1)\right)^2}\right)C_2^{\mu},
$$

and

$$\begin{aligned} B &= \mu\left(\frac{\Gamma(2\mu+1)-(\Gamma(\mu+1))^2}{\mu(\Gamma(\mu+1))^2}\right)^{\mu-1} \\ &\quad C_2^{\mu-1}\left(\frac{1}{\mu}\left(\frac{\Gamma(3\mu+1)-\Gamma(2\mu+1)(\Gamma(\mu+1))}{(\Gamma(2\mu+1))}C_3+\Gamma(2\mu+1)\frac{(\Gamma(\mu+1))^2-\Gamma(2\mu+1)}{(\Gamma(\mu+1))^3}\right.\right. \\ &\quad \left.\left.C_2^2\right)\right)+\frac{1}{2\mu}\left(1-\frac{1}{\mu}\right)\left(\frac{(\Gamma(\mu+1))^2-\Gamma(2\mu+1)^2}{(\Gamma(\mu+1))^4}C_2^2\right). \end{aligned}$$

3. Numerical Results

In this section, we aim to demonstrate the power, effectiveness, performance, and convergence behavior of the proposed iterative scheme (2. 1) by applying it to several numerical test problems. A comparison of the resulting numerical outcomes with those obtained from previously established methods will also be provided, focusing on the region near the roots to highlight the advantages of the new approach.

Giro Candelario [5] extended the concept of a single-step fractional iterative process in 2019 to a two-step procedure. He devised a two-step approach that requires one function and one fractional derivative value of a function $\Psi(\eta)$ of order α in order to reach the $(2\alpha+1)th$ order of convergence.

$$\begin{aligned} \acute{Y_t} &= \eta_t - \left(\Gamma(\mu+1)\frac{\Psi(\eta_t)}{cD_{\eta^-}^{\mu}\Psi(\eta_t)}\right)^{1/\mu}, t=0,1,2,..., \\ \eta_{t+1} &= \acute{Y_t} - \left(\Gamma(\mu+1)\frac{\Psi(\acute{Y_t})}{cD_{\eta^-}^{\mu}\Psi(\eta_t)}\right)^{1/\mu}, t=0,1,2,..., \end{aligned} \tag{3. 21}$$

where $cD_{\eta^-}^{\mu}\Psi(\eta_t)$ represents the Caputo fractional derivative of order μ and $0<\mu\leq 1$.

Comparison has been made on the basis of number of iteration indicated as t, the function value at η_t, that is $|\Psi(\eta_t)|$, the absolute error at each iteration $|\eta_t-\eta_{t+1}|$. Tables 1-4 shows the comparison of our presented methods M_SFR with the existing methods CFT given in [5]. Wolfram Mathematica 8 and Maple 22, two programming packages, were used for all of the computational work. To reduce the round of error, we perform our computations with multiple significant digits (minimum 1000 number of significant digits). Due to limitations, we are only able to present the results as a table with up to few decimal places.

In addition, we have compared the presented scheme with the existing ones by selecting few real-life problems along with their exact root and initial guess η_0 are listed below in Tables 1-4.

Example 3.1. ***Civil Engineering Application***

A beam with uniform characteristics and length L is simply supported at the left end and clamped to the wall at the right end, with loads rising uniformly across the beam. Because of the loads the beam's Y-shaped deflection will be displayed as the blue lines. The beam

shows greatest deflection when weight is introduced. The nonlinear method can be used to determine deflection Y, or the resultant deflection curve.

$$y = \frac{w_0}{120EIL}\left(-\eta^5 + 2L^2\eta^3 - L^4\eta\right) \tag{3. 22}$$

where E represents the beam's elasticity, I denotes its inertia, and L denotes its length. $f'(\eta) = 0$, that is, in order to determine the greatest deflection.

$$\frac{w_0}{120EIL}\left(-5\eta^4 + 6L^2\eta^2 - L^4\right) = 0$$

or

$$\Psi_1(\eta) = \frac{w_0}{120EIL}\left(-5\eta^4 + 6L^2\eta^2 - L^4\right) \tag{3. 23}$$

This nonlinear equation is used to determine the beam's maximum deflection under load. The location of maximal deflection will be provided by the η approximation. Where $w_0 = 2.5\,kN/cm, L = 600\,cm, E = 50,000\,kN/cm^3$, and $I = 30,000\,cm^4$. $\eta_1 = -599.999$, $\eta_2 = -268.328$, $\eta_3 = 268.328$, and $\eta_4 = 599.999$ are the four real roots of equation (3. 23). Using an initial approximation of $\eta_0 = -267$, we will estimate the root $\eta_2 = -268.328$.

$\Psi_1(\eta) = \frac{w_0}{120EIL}\left(-5\eta^4 + 6L^2\eta^2 - L^4\right),\ \eta_0 = -267$				
μ	*Method*	$\lvert\eta_{t+1} - \eta_t\rvert$	$\lvert\Psi(\eta_t)\rvert$	t
0.50	M_SFR	0.062641	3.792630×10^{18}	*19*
	M_CFT	0.072770	3.939387×10^{18}	*19*
0.60	M_SFR	0.000011	3.428976×10^{16}	*19*
	M_CFT	0.000011	3.429003×10^{16}	*19*
0.70	M_SFR	0.000393	3.633460×10^{16}	*19*
	M_CFT	0.000393	3.634185×10^{16}	*19*
0.80	M_SFR	0.000096	4.431137×10^{15}	*19*
	M_CFT	0.000096	4.431137×10^{15}	*19*
0.90	M_SFR	0.000002	3.640474×10^{13}	*19*
	M_CFT	0.000002	3.640474×10^{13}	*19*
0.99	M_SFR	$0.000000 + 0.000000i$	1.804343×10^{11}	*19*
	M_CFT	$0.000000 + 0.000000i$	1.804343×10^{11}	*19*

TABLE 1. Convergence behavior of M_SFR and M_CFT methods for $\Psi_1(\eta)$ at selected values of μ.

Table 1 illustrates that SFRM1 outperforms CFT both in terms of absolute error and functional evaluation.

Example 3.2. ***Bacterial Growth Problem***

When a bacterial population increases exponentially with time. A population at every given moment t can be represented by the formula

$$P(t) = P_0 exp(rt),$$

where P_0 is the initial population size and $P(t) = P_0 exp(rt)$. We call this growth rate r. Now is the moment to determine when the population size hits a specific critical point,

which we will simply set as $P(t) = P_0 + 1$. This indicates a precise one-unit rise in the population. Let's begin with the equation:

$$P(t) = P_0 exp(rt) = P_0 + 1$$

We determine its value to be

$$P_0 exp(rt) = P_0 + 1$$

Dividing by P_0 (as a whole number):

$$exp(rt) = 1 + \frac{1}{P_0}$$

In cases where P_0 is large, $\frac{1}{P_0}$ is very small, and if we assume it to be insignificant for the sake of simplicity, we obtain:

$$exp(rt) \approx 1.$$

Consequently, the simplified equation:

$$exp(rt) - 1 = 0.$$

Let $\eta = rt$, we get

$$exp(\eta) - 1 = 0$$

and

$$\Psi_2(\eta) = exp(\eta) - 1 \tag{3. 24}$$

The results for our second test function are listed below in Table 2:

$\Psi_2(\eta) = \exp(\eta) - 1,\ \eta_0 = 0.1$				
μ	*Method*	$\lvert\eta_{t+1} - \eta_t\rvert$	$\lvert\Psi(\eta_t)\rvert$	t
0.5	M_SFR	2.500000×10^{-3}	3.100000×10^{-2}	*19*
	M_CFT	2.550241×10^{-3}	4.003806×10^{-2}	*19*
0.6	M_SFR	1.785603×10^{-3}	1.543270×10^{-2}	*19*
	M_CFT	1.772110×10^{-3}	1.544641×10^{-2}	*19*
0.7	M_SFR	7.213910×10^{-4}	3.761200×10^{-3}	*19*
	M_CFT	7.200161×10^{-4}	3.762584×10^{-3}	*19*
0.8	M_SFR	1.263790×10^{-4}	3.771487×10^{-4}	*19*
	M_CFT	1.263541×10^{-4}	3.771736×10^{-4}	*19*
0.9	M_SFR	2.286687×10^{-6}	3.039176×10^{-6}	*19*
	M_CFT	2.286683×10^{-6}	3.039179×10^{-6}	*19*
0.99	M_SFR	0.000000×10^{0}	2.136654×10^{0}	*19*
	M_CFT	0.000000×10^{0}	2.136654×10^{0}	*19*

TABLE 2. Convergence behavior of M_SFR and M_CFT methods for $\Psi_2(\eta)$.

Table 2 illustrates that SFRM1 outperforms CFT both in terms of absolute error and functional evaluation.

Example 3.3. ***Chemical Sciences***

The acidity of a solution of MgOH in HCl may be calculated using the formula

$$\frac{3.64 \times 10^{-11}}{[H_3O^+]} = [H_3O^+] + 3.6 \times 10^{-4},$$

where HCl is hydrochloric acid and [H3O+] is the concentration of hydronium ions. By taking

$$\eta = 10^4[H3O+],$$

we obtain the following nonlinear model:

$$\Psi_3(\eta) = \eta^3 + 3.6\eta^2 - 36.4 \tag{3. 25}$$

has two complex conjugate roots $-3 \pm 2.3i$ *and one real root* 2.4 *as shown in the figure. Using 128-digit floating point arithmetic, we have approximated our desired real root* 2.4 *with initial guess* β *by taking* $\in = 10^{-10}$.

$\Psi_3(\eta) = \eta^3 + 3.6\eta^2 - 36.4, \quad \eta_0 = 2.39$				
μ	*Method*	$\lvert\eta_{t+1} - \eta_t\rvert$	$\lvert\Psi(\eta_t)\rvert$	i
0.5	M_SFR	2.900000×10^{-1}	2.095000×10^{1}	19
	M_CFT	6.389930×10^{-1}	2.719127×10^{1}	19
0.6	M_SFR	$1.132325 \times 10^{-3} - 7.282846 \times 10^{-3}i$	1.234009×10^{0}	19
	M_CFT	$1.201565 \times 10^{-3} - 7.179305 \times 10^{-3}i$	1.234792×10^{0}	19
0.7	M_SFR	$7.053230 \times 10^{-4} - 1.105709 \times 10^{-3}i$	1.998612×10^{-1}	19
	M_CFT	$7.056430 \times 10^{-4} - 1.101989 \times 10^{-3}i$	1.999330×10^{-1}	19
0.8	M_SFR	$1.176570 \times 10^{-4} + 1.189395 \times 10^{-4}i$	1.667992×10^{-2}	19
	M_CFT	$1.656980 \times 10^{-4} + 1.024818 \times 10^{-4}i$	1.866591×10^{-2}	19
0.9	M_SFR	$1.929000 \times 10^{-6} + 1.648112 \times 10^{-6}i$	1.187384×10^{-4}	19
	M_CFT	$2.564000 \times 10^{-6} + 1.571901 \times 10^{-6}i$	1.370688×10^{-4}	19
0.99	M_SFR	$0 - 5.0754 \times 10^{-17}i$	6.954933×10^{-9}	19
	M_CFT	$0 - 5.0756 \times 10^{-17}i$	6.954933×10^{-9}	19

TABLE 3. Convergence behavior of M_SFR and M_CFT methods for $\Psi_3(\eta)$.

.

From Table 3, M_SFR exhibits lower error and provides better functional evaluations.

Example 3.4. *Let us consider the standard nonlinear test function:*

$$\Psi_4(\eta) = \eta^4 + 4\eta^3 - 24\eta^2 + 16\eta + 16 \tag{3. 26}$$

The numerical results for the test function $\Psi_4(\eta)$ *are depicted in Table 4*

Table 4 clearly demonstrates that M_SFR *performs better than* M_CFT *in terms of both functional evaluation and absolute error.*

Table 1 demonstrate that the convergence behavior of the recently developed techniques beats the known, existing solutions for the test problem $\Psi_1(\eta)$. *The absolute error is smaller than that of the approved, in-use* CFT *techniques at this time. Furthermore,*

$\Psi_4(\eta) = \eta^4 + 4\eta^3 - 24\eta^2 + 16\eta + 16$, $\eta_0 = 2.5$				
μ	*Method*	$\lvert\eta_{t+1} - \eta_t\rvert$	$\lvert\Psi(\eta_t)\rvert$	i
0.5	M_SFR	-1.257345×10^{-2}	8.233089×10^{-1}	19
	M_CFT	-1.210865×10^{-2}	8.278105×10^{-1}	19
0.6	M_SFR	-9.809610×10^{-3}	1.965935×10^{-1}	19
	M_CFT	-9.623972×10^{-3}	1.974364×10^{-1}	19
0.7	M_SFR	-5.810046×10^{-3}	2.875596×10^{-2}	19
	M_CFT	-5.767616×10^{-3}	2.882772×10^{-2}	19
0.8	M_SFR	2.296984×10^{-3}	1.741169×10^{-3}	19
	M_CFT	2.293024×10^{-3}	1.742795×10^{-3}	19
0.9	M_SFR	3.776780×10^{-4}	1.377282×10^{-5}	19
	M_CFT	3.776280×10^{-4}	1.377464×10^{-5}	19
0.99	M_SFR	$2.965300 \times 10^{-5} + 6.746837 \times 10^{-7}i$	1.516733×10^{-9}	19
	M_CFT	$2.965300 \times 10^{-5} + 6.746813 \times 10^{-7}i$	1.516733×10^{-9}	19

TABLE 4. Convergence behavior of M_SFR and M_CFT methods for $\Psi_4(\eta)$.

method M_SFR outperforms other CFT techniques. Table 2 shows that the newly proposed method M_SFR outperforms the existing methods CFT for the test function $\Psi_2(\eta)$. M_SFR is responsible for the lower absolute inaccuracy. Table 3 show that the newly developed technique performs better than the strategies previously discussed. However, the CFT values for the test function $\Psi_3(\eta)$ are similar to those of M_SFR. Table 4 clearly show that the newly proposed methods M_SFR outperform CFT for function $\Psi_4(\eta)$.

4. DYNAMICAL ANALYSIS

The region in the complex plane where various initial guesses converge to certain roots of a given function under an iterative technique is referred to as a basin of attraction in root-finding issues. Important insights into the operation of iterative algorithms, particularly with regard to patterns of convergence and divergence, are provided by visualization. It is possible to adequately illustrate the stability and convergence zones of iterative systems by using sophisticated techniques such as symmetric basins of attraction. Refer to [7] and [14] for thorough descriptions of the complex behavior and fundamental concepts of rational functions. The dynamical portraits produced by my proposed method and a previously established method are compared in this section with the aim of proving that my method has a more stable convergence behavior with a significantly smaller divergence region, which leads to a more dependable solution approach.

We used a classic root-finding issue involving a function with numerous roots in the complex plane to create the basin of attraction for both approaches. For each technique, an iterative dense grid of starting points was employed. Each point was color-coded according to the root it converged to once the corresponding iterative procedures were applied, resulting in the basin of attraction. We performed this analysis on few real-world problems and selected test functions to examine and evaluate the stability of methods more thoroughly. The table below lists these functions along with their exact roots.

Function	Roots
$\Psi_1(\eta) = \eta^3 + 3.6\eta^2 - 36.4$	$-3 \pm 2.3i$, 2.4
$\Psi_2(\eta) = \eta^4 + 4\eta^3 - 24\eta^2 + 16\eta + 16$	-2, -2, 2, 2
$\psi_3(\eta) = \eta^4 - 10\eta^2 + 9$	± 1, ± 3
$\psi_4(\eta) = \eta^5 - 1$	1, $e^{i\frac{2\pi}{5}} = \cos\left(\frac{2\pi}{5}\right) + i\sin\left(\frac{2\pi}{5}\right)$, $e^{i\frac{4\pi}{5}} = \cos\left(\frac{4\pi}{5}\right) + i\sin\left(\frac{4\pi}{5}\right)$, $e^{i\frac{6\pi}{5}} = \cos\left(\frac{6\pi}{5}\right) + i\sin\left(\frac{6\pi}{5}\right)$, $e^{i\frac{8\pi}{5}} = \cos\left(\frac{8\pi}{5}\right) + i\sin\left(\frac{8\pi}{5}\right)$
$\Psi_5(\eta) = -12.84\eta^6 - 25.6\eta^5 + 16.55\eta^4$ $-2.21\eta^3 + 26.71\eta^2 - 4.29\eta - 15.21$	$0.82366 + 0.24769i$, $0.82366 - 0.24769i$, -2.62297, -0.584, $-0.21705 + 0.99911i$, $-0.21705 - 0.99911i$

TABLE 5. Nonlinear test functions and their roots

Here, we use fractional iterative strategies to examine the symmetric basins of attraction. Numerical analysis provides important insights into the stability of iterative procedures and relates them to complex properties of rational functions. We used Matlab $R2018a$ to create symmetric basins of attraction using two distinct strategies. We looked at a grid with a square box that was 400×400 and $B = [-2, 2] \times [-2, 2] \subset \mathbb{C}$.

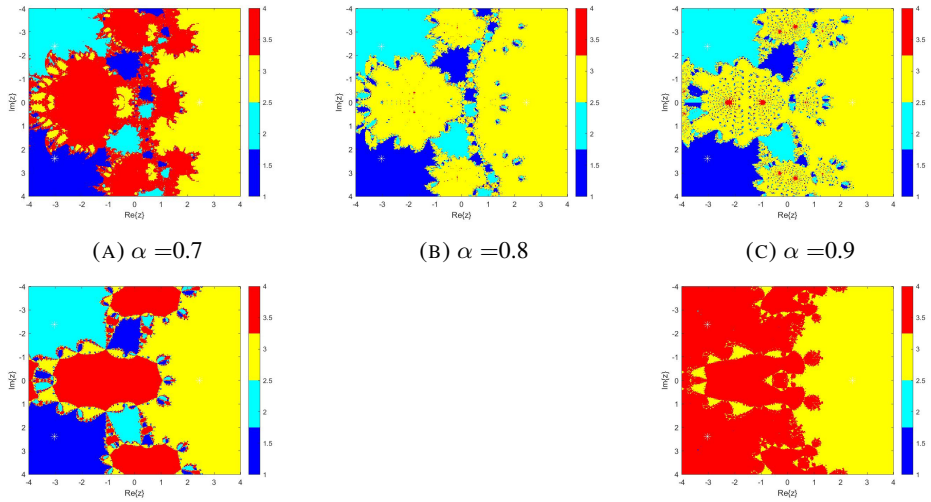

(A) α =0.7 (B) α =0.8 (C) α =0.9

(D) α =1.0 (E) α =1.1

FIGURE 1. Basin of attraction of M_SFR for $\Psi_1(\eta)$

Figure 1 illustrates the basin of attraction for the M_SFR method applied to $\Psi_1(\eta)$. A basin of attraction represents the regions in the complex plane where the iterative root-finding method converges to specific roots of the function $\Psi_1(\eta)$. The different colors in

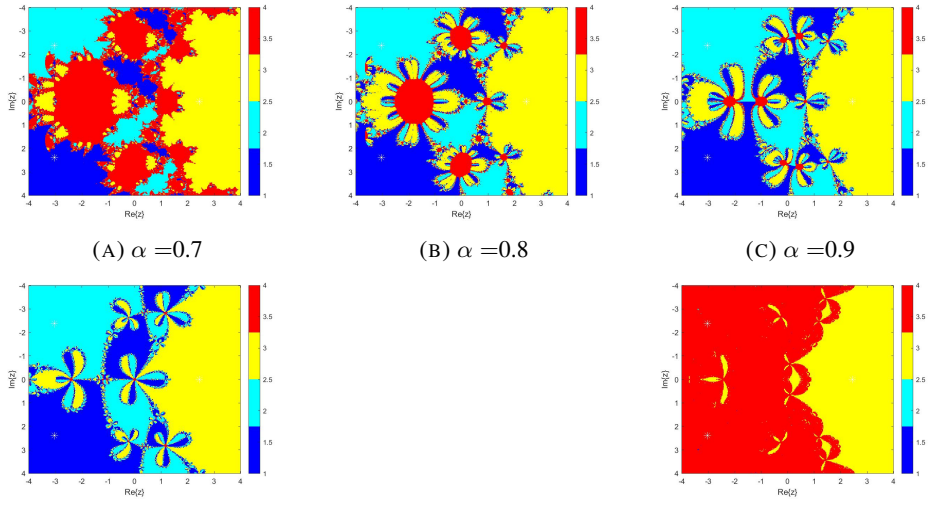

(A) α =0.7 (B) α =0.8 (C) α =0.9

(D) α =1.0 (E) α =1.1

FIGURE 2. Basin of attraction of M_CFT for $\Psi_1(\eta)$

the plot correspond to distinct roots, and the boundaries between regions indicate sensitive dependence on initial conditions, highlighting the chaotic behavior in those areas. The M_SFR method demonstrates a structured convergence pattern, with relatively sharp and distinct regions, especially for larger values of α.

Figure 2 presents the basin of attraction for the M_CFT method applied to $\Psi_1(\eta)$. Similar to the M_SFR method, the basins here also indicate convergence to specific roots of $\Psi_1(\eta)$ based on initial conditions. However, the M_CFT method exhibits differences in the shape and distribution of the basins, particularly near the boundaries. The convergence regions are more intricate, and the boundaries between basins show a higher level of fractal-like detail for certain values of α.

By comparing the two methods, we observe that M_SFR generally produces smoother and more defined basins of attraction, indicating more predictable convergence behavior. In contrast, M_CFT generates more complex basin structures, which may suggest greater sensitivity to initial conditions. These comparisons highlight the trade-offs between the two methods in terms of stability and predictability for solving $\Psi_1(\eta)$ in the complex plane.

Figure 3 illustrates the basin of attraction for the M_SFR method applied to $\Psi_2(\eta)$. Similar to Figure 1, the basin of attraction represents the regions in the complex plane where the iterative root-finding method converges to specific roots of $\Psi_2(\eta)$. The distinct colors correspond to the convergence toward different roots, while the boundaries between regions signify areas of high sensitivity to initial conditions. The M_SFR method demonstrates well-structured and relatively symmetric basins of attraction, with the regions becoming sharper and more defined as α increases. This indicates predictable convergence behavior for $\Psi_2(\eta)$ under this method.

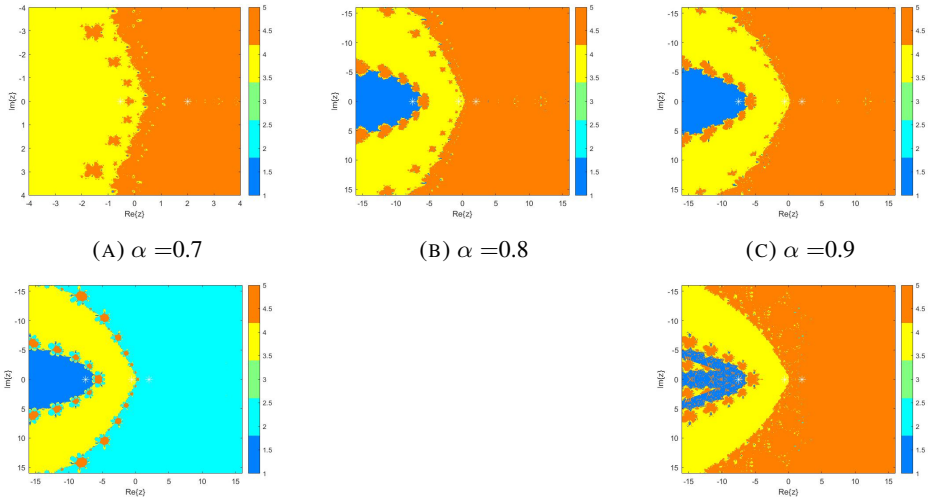

(A) α =0.7 (B) α =0.8 (C) α =0.9

(D) α =1.0 (E) α =1.1

FIGURE 3. Basin of attraction of M_SFR for $\Psi_2(\eta)$

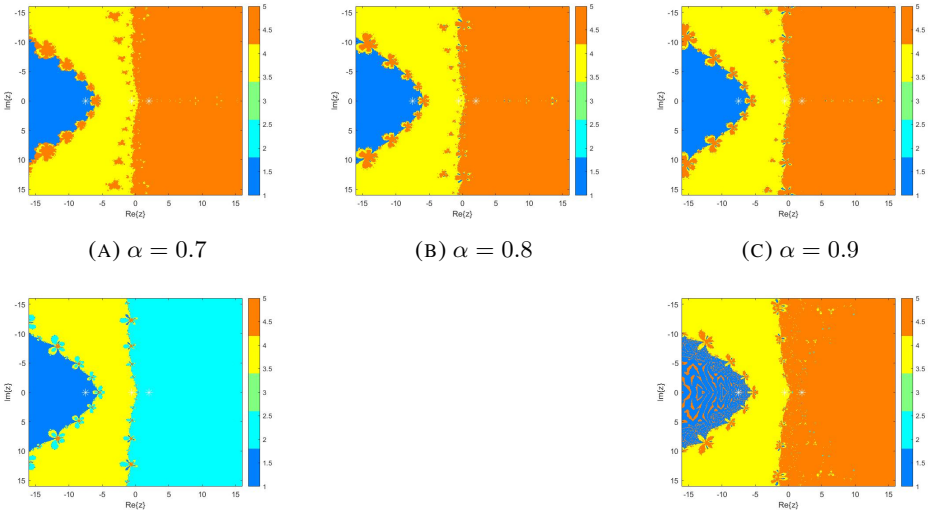

(A) $\alpha = 0.7$ (B) $\alpha = 0.8$ (C) $\alpha = 0.9$

(D) $\alpha = 1.0$ (E) $\alpha = 1.1$

FIGURE 4. Basin of attraction of M_CFT for $\Psi_2(\eta)$

Figure 4 presents the basin of attraction for the M_CFT method applied to $\Psi_2(\eta)$. The structure of the basins here also reveals convergence to specific roots of $\Psi_2(\eta)$, with varying complexity across different values of α. Compared to M_SFR, the M_CFT

method shows a more intricate and fragmented pattern near the boundaries, particularly for smaller values of α. This suggests that M_CFT may exhibit greater sensitivity to initial conditions for $\Psi_2(\eta)$, especially in regions close to the boundaries of convergence.

By comparing Figures 3 and 4, it is evident that M_SFR offers more uniform and smoother basins of attraction for $\Psi_2(\eta)$, which may make it more reliable for certain applications. On the other hand, M_CFT provides more complex boundary behavior, which could be advantageous in capturing finer details of convergence dynamics but may also indicate a trade-off in stability and predictability. The differences highlight the strengths and weaknesses of both methods for solving $\Psi_2(\eta)$ in the complex plane.

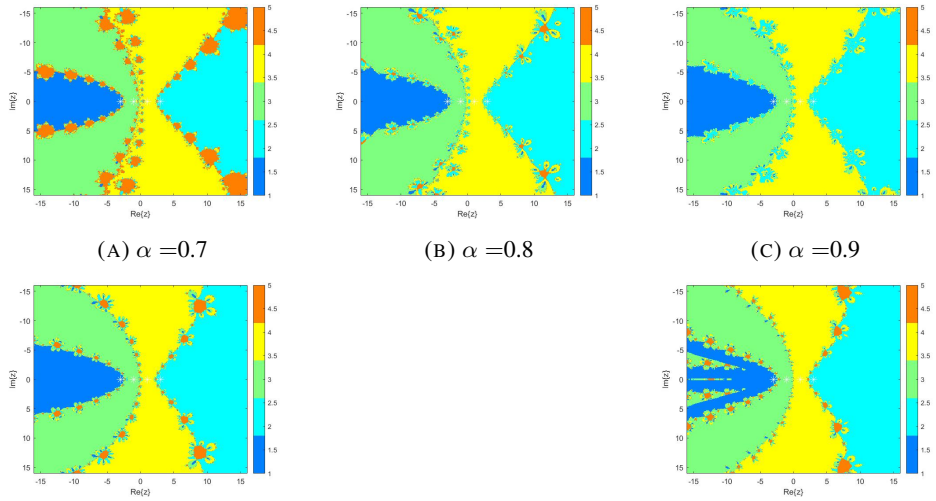

(A) α =0.7 (B) α =0.8 (C) α =0.9

(D) α =1.0 (E) α =1.1

FIGURE 5. Basin of attraction of M_SFR for $\Psi_3(\eta)$

Figure 5 illustrates the basin of attraction for the M_SFR method applied to $\Psi_3(\eta)$. The basins of attraction represent regions in the complex plane where the iterative root-finding method converges to specific roots of $\Psi_3(\eta)$. Each distinct color corresponds to convergence to a particular root, while the boundaries signify regions of higher sensitivity to initial conditions. The M_SFR method demonstrates symmetric and well-defined basins, particularly as α increases. For lower values of α, the basins exhibit slight irregularities near the boundaries, but the convergence regions remain clearly distinguishable overall. This reflects predictable and stable behavior under the M_SFR method for $\Psi_3(\eta)$.

Figure 6 shows the basin of attraction for the M_CFT method applied to $\Psi_3(\eta)$. The convergence regions are still represented by distinct colors corresponding to the roots of $\Psi_3(\eta)$. However, compared to M_SFR, the M_CFT method exhibits slightly more intricate and fragmented patterns along the basin boundaries, especially for smaller values of α. As α increases, the basins become smoother, but the method still retains more complex boundary behavior compared to M_SFR. This indicates that M_CFT may be more sensitive to initial conditions in certain regions of the complex plane.

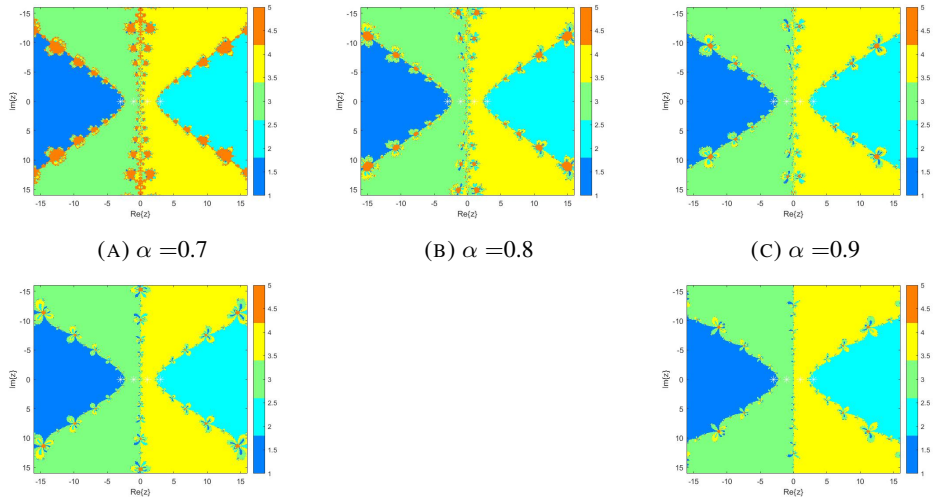

(A) α =0.7 (B) α =0.8 (C) α =0.9

(D) α =1.0 (E) α =1.1

FIGURE 6. Basin of attraction of M_CFT for $\Psi_3(\eta)$

By comparing Figures 5 and 6, it is evident that M_SFR provides more consistent and structured basins of attraction for $\Psi_3(\eta)$, which may be advantageous in terms of stability and predictability. In contrast, M_CFT reveals more detailed and intricate basin boundaries, which could offer insights into convergence dynamics but may come at the cost of increased sensitivity to initial conditions. These comparisons highlight the differences between the two methods when applied to $\Psi_3(\eta)$, providing insight into their respective strengths and limitations.

Figure 7 illustrates the basin of attraction for the M_SFR method applied to a function with five distinct roots. The basins of attraction represent the regions in the complex plane where the iterative root-finding method converges to one of the five roots. Each color corresponds to convergence to a specific root, while the intricate boundaries between regions signify areas of high sensitivity to initial conditions. The M_SFR method demonstrates a symmetric and organized structure for the basins, particularly as α increases. For smaller values of α, the regions near the boundaries show slight irregularities, but overall, the convergence patterns remain stable and predictable. The method's clear delineation of basins reflects its reliability for this complex scenario.

Figure 8 shows the basin of attraction for the M_CFT method applied to the same function with five roots. Similar to M_SFR, the basins represent regions converging to different roots, with each root marked by a unique color. However, the M_CFT method exhibits more intricate and fragmented patterns along the basin boundaries, especially for smaller values of α. These complex patterns indicate that the M_CFT method may be more sensitive to initial conditions in certain regions. As α increases, the basins become smoother, but the method retains more chaotic behavior near the boundaries compared to M_SFR.

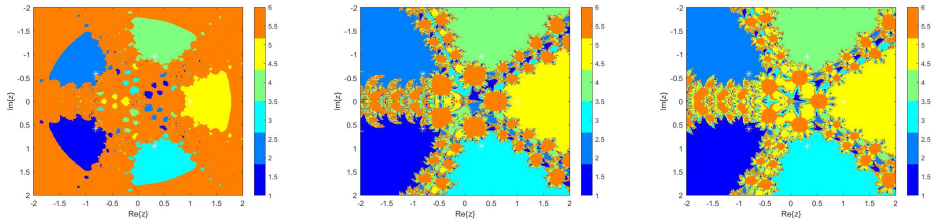

(A) α =0.6 (B) α =0.7 (C) α =0.8

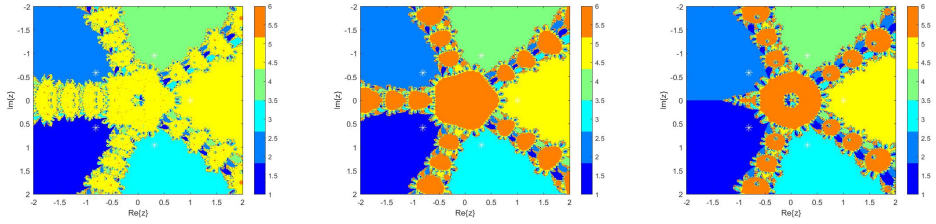

(D) α =0.9 (E) α =1.0 (F) α =1.1

FIGURE 7. Basin of attraction of M_SFR for $\Psi_4(\eta)$

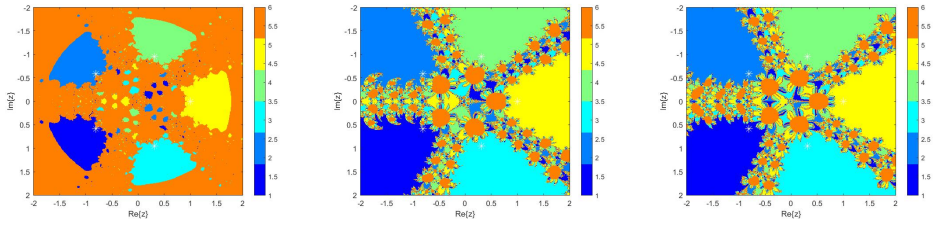

(A) α =0.6 (B) α =0.7 (C) α =0.8

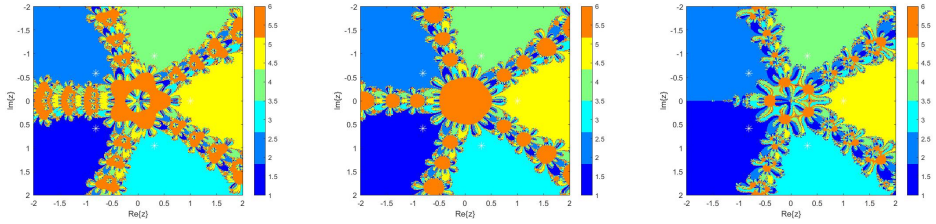

(D) α =0.9 (E) α =1.0 (F) α =1.1

FIGURE 8. Basin of attraction of M_CFT for $\Psi_4(\eta)$

By comparing Figures 7 and 8, we observe that M_SFR provides more stable and structured basins of attraction for a function with five roots, making it well-suited for applications requiring predictable convergence behavior. On the other hand, M_CFT captures

more detailed and intricate basin boundaries, which may provide deeper insights into the convergence dynamics but at the cost of increased sensitivity and potential instability in certain regions. The comparison highlights the trade-offs between the two methods when applied to functions with multiple roots, offering insights into their suitability for different scenarios.

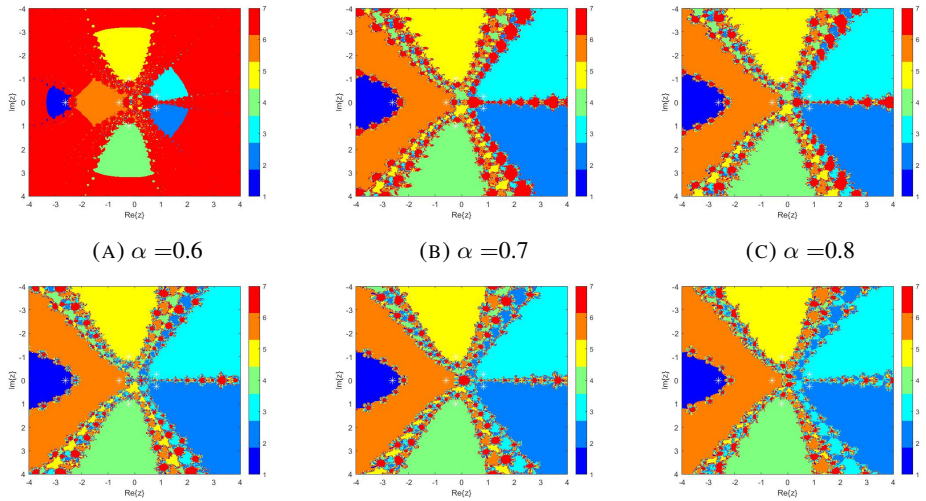

(A) α =0.6 (B) α =0.7 (C) α =0.8

(D) α =0.9 (E) α =1.0 (F) α =1.1

FIGURE 9. Basin of attraction of M_SFR for $\Psi_5(\eta)$

Figure 9 illustrates the basin of attraction for the M_SFR method applied to a function with six roots. The basins of attraction represent regions in the complex plane where the iterative method converges to one of the six roots. Each distinct color corresponds to convergence toward a specific root, and the boundaries between the basins mark areas of high sensitivity to initial conditions. For the M_SFR method, the basins are symmetric and exhibit clear separation between convergence regions. As α increases, the basins become more well-defined, with reduced irregularities near the boundaries. This demonstrates the stability and efficiency of the M_SFR method for solving functions with multiple roots.

Figure 10 presents the basin of attraction for the M_CFT method applied to the same function with six roots. Similar to M_SFR, each color represents convergence to one of the six roots. However, the M_CFT method shows more intricate and fractal-like boundary patterns, particularly for smaller values of α. As α increases, the convergence regions become more structured, but the boundaries remain more detailed compared to the M_SFR method. This suggests that while M_CFT is capable of capturing finer details in the basin structure, it may also exhibit greater sensitivity to initial conditions, especially near the boundary regions.

By comparing Figures 9 and 10, it is evident that the M_SFR method provides smoother and more predictable basins of attraction for functions with six roots. In contrast, the M_CFT method produces more complex and intricate boundaries, which may offer deeper

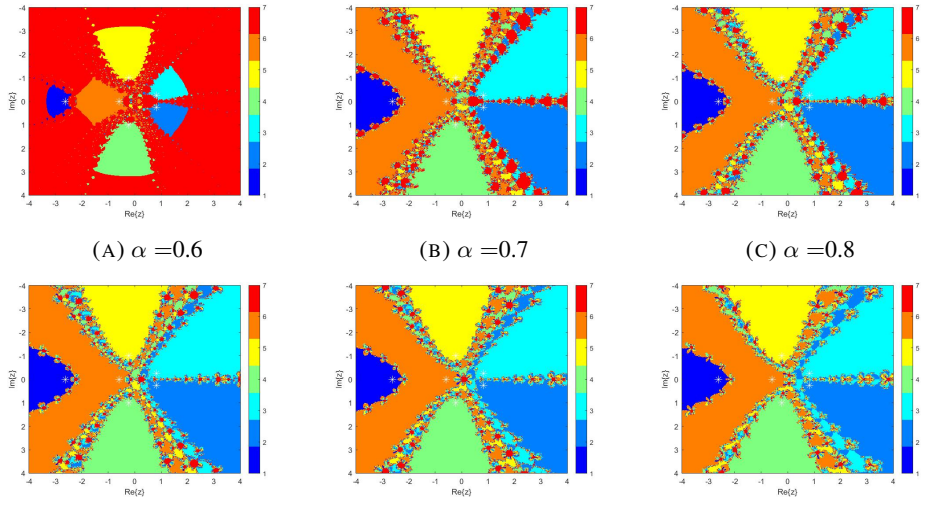

(A) α =0.6 (B) α =0.7 (C) α =0.8

(D) α =0.9 (E) α =1.0 (F) α =1.1

FIGURE 10. Basin of attraction of M_CFT for $\Psi_5(\eta)$

insights into the dynamics of convergence but may also result in less stability in certain regions. These observations highlight the trade-offs between the two methods in terms of stability, sensitivity, and the ability to handle functions with multiple roots.

Numerous solutions that could have a big impact on the system under study are also revealed by looking at the basins of attraction. Thus, researching attraction basins is a useful way to understand the behavior of iterative processes and make them more efficient. This approach can make complex problems easier and faster to handle for experts and researchers in a variety of sectors.

The dynamical profiles of the two approaches demonstrate how much better the suggested approach performs in terms of stability and convergence. The suggested technique demonstrates increased accuracy and efficiency for root-finding issues by decreasing the divergence zones and generating more distinct basins of attraction.

5. CONCLUSION

In this study, we apply the idea of fractional derivative to each current iterative scheme substep. There is a lack of two-step fractional iterative methods in the literature, with only a few single-step fractional iterative methods available and just one existing two-step method. Recognizing the need for further development in this area, we have developed a new two-step fractional iterative scheme that provides improved results compared to the previously available method. Riemann-Liouville and Caputo fractional derivatives have been used in recent advances in fractional Newton techniques. We developed two-step methods that utilize the Riemann-Liouville fractional derivative as well as the Caputo fractional derivative. In the unlikely case that the circumstance is more complicated than normal, these approaches are intended to handle issues. To verify their validity, we subjected

them to numerical testing and assessed their convergence with regard to practical applications such chemical research, civil engineering, restroom enterprises, and bridge beam deflection.The comparative findings shown in Tables 1-4 show that the recently created schemes, M_SFR, outperform M_CFT with better results. The basin of attraction indicates that the M_SFR method outperforms the M_CFT method, particularly in scenarios that require highly sensitive iterative approaches. M_SFR demonstrates a range of intricate basin configurations, especially as the parameter α varies. This adaptability can be beneficial when aiming to capture complex dynamics.

AUTHORS' CONTRIBUTION

Conceptualization: Saima Akram, Rida Batool, and Faiza Akram; Problem formulation: Saima Akram, Rida Batool, and Faiza Akram; Methodology: Rida Batool, and Faiza Akram; Formal Analysis: Saima Akram, and Faiza Akram; Writing original draft: Rida Batool; Investigation: Saima Akram, and Faiza Akram; Validation: Saima Akram, and Faiza Akram; Software: Saima Akram, Rida Batool, and Faiza Akram; Visualization: Rida Batool, and Faiza Akram; Supervision: Saima Akram; Review and Editing: Saima Akram, and Faiza Akram. All authors have read and agreed to the published version of the manuscript.

ACKNOWLEDGMENTS

The authors would like to thank the anonymous reviewers for their valuable comments, which have improved the final version of this manuscript.

FUNDING

This research received no external funding.

CONFLICT OF INTEREST

The authors declare no conflicts of interest regarding the publication of this paper.

REFERENCES

[1] A. Akgül, A. Cordero, and J.R. Torregrosa, *A fractional Newton method with* 2α*th-order of convergence and its stability*, Appl. Math. Lett. **98** (2019), 344–351.

[2] T.M. Atanackovic, S. Pilipovic, B. Stankovic, and D. Zorica, *Fractional calculus with applications in mechanics: wave propagation, impact and variational principles*, John Wiley & Sons, (2014).

[3] D. Baleanu and B. Shiri, *Numerical methods for solving systems of Atangana-Baleanu fractional differential equations*, in Applications of Fractional Calculus to Modeling in Dynamics and Chaos, (2022), 353–378.

[4] M.A. Bayrak, A. Demir, and E. Ozbilge, *On fractional Newton-type method for nonlinear problems*, J. Math. **2022**(1) (2022), 7070253.

[5] G. Candelario, A. Cordero, and J.R. Torregrosa, *Multipoint fractional iterative methods with* $(2\alpha + 1)$*th-order of convergence for solving nonlinear problems*, Mathematics **8**(3) (2020), 452.

[6] F. Cajori, *Historical note on the Newton–Raphson method of approximation*, Amer. Math. Monthly **18**(2) (1911), 29–32.

[7] C. Chun and B. Neta, *Comparing the basins of attraction for Kanwar–Bhatia–Kansal family to the best fourth order method*, Appl. Math. Comput. **266** (2015), 277–292.

[8] R. Hilfer (Ed.), *Applications of fractional calculus in physics*, World Scientific, (2000).

[9] G. Jumarie, *Modified Riemann–Liouville derivative and fractional Taylor series of nondifferentiable functions: further results*, Comput. Math. Appl. **51**(9–10) (2006), 1367–1376.

[10] Z.M. Odibat and N.T. Shawagfeh, *Generalized Taylor's formula*, Appl. Math. Comput. **186**(1) (2007), 286–293.

[11] M. Shams and B. Carpentieri, *Efficient inverse fractional neural network-based simultaneous schemes for nonlinear engineering applications*, Fractal Fract. **7**(12) (2023), 849.

[12] M. Shams and B. Carpentieri, *On highly efficient fractional numerical method for solving nonlinear engineering models*, Mathematics **11**(24) (2023), 4914.

[13] M. Shams, N. Kausar, P. Agarwal, S. Jain, M.A. Salman, and M.A. Shah, *On family of the Caputo-type fractional numerical scheme for solving polynomial equations*, Appl. Math. Sci. Eng. **31**(1) (2023), 2181959.

[14] J.R. Sharma and S. Kumar, *Efficient methods of optimal eighth and sixteenth order convergence for solving nonlinear equations*, SeMA J. **75** (2018), 229–253.